Sub-barrier fusion of ^{37}Cl with ^{58,60,62,64}Ni

J. J. Vega,* E. F. Aguilera, and G. Murillo
Instituto Nacional de Investigaciones Nucleares, Apartado Postal 18-1027, Mexico, Distrito Federal 11800, Mexico

J. J. Kolata, A. Morsad,† and X. J. Kong‡
Department of Physics, University of Notre Dame, Notre Dame, Indiana 46556
(Received 27 November 1989)

Near-barrier and sub-barrier fusion excitation functions have been measured for the ^{37}Cl+^{58,60,62,64}Ni systems using a recoil velocity spectrometer to identify evaporation residues. A considerable amount of enhancement was observed for all systems studied. The measured excitation functions for ^{37}Cl+^{58,62,64}Ni are not in agreement with published results for these systems. The data were analyzed in the context of a coupled-channels model which took into account either the dependence of the fusion cross section on the coupling to surface vibrational modes, or, alternatively, on the orientation of deformed colliding nuclei. Very good agreement was obtained with the experimental data under the assumption that ^{37}Cl exhibits a moderate oblate static deformation, while the light Ni isotopes are spherical vibrators. On the other hand, the data for ^{37}Cl+^{64}Ni favor a moderate static oblate deformation for ^{64}Ni.

I. INTRODUCTION

The tunneling of charged particles through the Coulomb barrier into the nuclear interior, eventually leading to a fusion, is a venerable problem in nuclear physics.[1] The interest in this subject has increased[2] considerably, however, since sub-barrier fusion was observed to present an unexpected enhancement with respect to the predictions of the simple one-dimensional models which accurately describe the above-barrier fusion data.[3] (See Ref. 4 for a review of this subject.) As a consequence of considerable theoretical effort exerted in attempting to explain these experimental results, a new dynamical picture of sub-barrier fusion has emerged. According to this new picture, additional degrees of freedom besides the one corresponding to the relative motion of the colliding nuclei are necessary and relevant components of the interaction potential that governs the fusion process at sub-barrier energies. Furthermore, these are internal degrees of freedom so that the nuclear reaction dynamics are strongly influenced by the underlying nuclear structure. It should therefore prove possible to extract nuclear structure information from sub-barrier fusion data, or conversely to determine the nature of the interaction if the structure is known.

It is within the above perspective that we decided to study the sub-barrier fusion of ^{37}Cl with ^{58,60,62,64}Ni. Our objective was to describe the measured fusion cross sections by including the effects of additional internal degrees of freedom, specifically, the coupling to surface vibrational modes or the orientational effects which results when one or more of the colliding nuclei exhibits a permanent deformation. In these calculations, furthermore, we used nuclear structure information taken from the literature with the idea that any remaining discrepancies between theory and experiment could then perhaps be ascribed to the influence of quasielastic transfer channels. However, as we shall see, it proved possible to explain all our results without invoking particle-transfer degrees of freedom.

The material presented in this paper is organized in the following way. A description of the experimental method is given in Sec. II. Next, in Sec. III the data are analyzed using a simple one-dimensional barrier penetration model, and then a description of the sub-barrier fusion is attempted by taking into account both orientational effects and coupling to surface vibrational modes. Finally, our conclusions are presented in Sec. IV.

II. EXPERIMENTAL METHOD

The experiments were performed using ^{37}Cl beams provided by the three-stage tandem Van de Graaff accelerator at the University of Notre Dame. Typical beam intensities of 1–4 particle nanomamperes (pnA) on target were obtained from a sputter ion source by using NaCl enriched in ^{37}Cl. The ^{58,60,64}Ni targets were self-supporting, but the ^{62}Ni target was evaporated onto a 20 μg/cm^2 C backing. All of the targets were enriched in the corresponding isotope. In order to determine their composition, we observed elastically scattered α particles at a bombarding energy of 12 MeV and a laboratory angle of 80° using a magnetic spectrograph. The target thicknesses were determined by measuring the energy loss of ^{16}O ions obtained by elastic scattering from ^{197}Au at a bombarding energy of 58 MeV. The results of these measurements are given in Table I.

The evaporation residues (ER) from fusion are emitted in a narrow cone within a few degrees around the beam axis, and their cross section is relatively small at energies below the barrier. Therefore, direct detection of residues becomes difficult in the presence of a large background arising from slit scattering and other similar types of events. To accomplish the separation, the evaporation

 ©1990 The American Physical Society

TABLE I. Composition of the targets used in this experiment. In each case, percentage figures refer to atomic percent.

Target	Thickness[a] ($\mu g/cm^2$)	Chemical and isotopic purity (%)	Principle contaminants (%)
^{58}Ni	187	>99.8	
^{60}Ni	220	>99.8	
^{62}Ni[b]	49	90.18(74)	0.67(7) ^{58}Ni 1.21(9) ^{60}Ni 7.94(7) ^{181}Ta
^{64}Ni	160	97.42(149)	0.99(14) ^{58}Ni 0.94(13) ^{60}Ni 0.66(11) ^{62}Ni

[a]Estimated ±7% uncertainty.
[b]Evaporated onto 20 $\mu g/cm^2$ C backing.

residues emerging from the target were deflected out of the direct beam by means of an electrostatic deflector. The value of the potential applied to the electrode plates was selected so as to maximize the yield from each target. The separated residues were then identified in a time-of-flight (TOF) and energy spectrometer, which consisted of a microchannel plate and a silicon-surface-barrier detector (SSB) which together defined a 1m flight path. The whole apparatus (TOF arm, electrostatic deflector and target chamber) was rigidly attached and designed to rotate as a unit, making it possible to measure the angular distribution over ±10° with respect to the beam. Preliminary descriptions of this spectrometer appear in Refs. 5 and 6. A more complete and detailed report will be the subject of a future publication.

For the systems studied in the present experiment, and in the energy range we are interested in, the ER cross section may be equated with the total fusion cross section since fission of the compound nucleus is negligible. Absolute differential cross sections were obtained by normalizing the ER yield to the elastic scattering cross section at forward angles, which is purely Rutherford. The elastic yield was measured with an array of four monitor counters symmetrically distributed with respect to the beam axis and at a laboratory angle of 15°. Due to the strong angular dependence of the Rutherford cross section at small angles, a high degree of precision (±0.01 mm) was achieved in determining the average beam position on target during a run. This corresponds to defining the average beam direction to ±0.01°, which is directly reflected in the high degree of precision (1%) obtained for the product of the integrated beam current times the target thickness in the present experiment. See Ref. 7 for a detailed description of this normalization procedure.

The transmission probability of the ER through the recoil velocity spectrometer was determined empirically by elastic scattering of ions of similar atomic and mass numbers, and kinetic energy. To accomplish this, we measured the Rutherford scattering of ^{103}Rh ions on ^{60}Ni at bombarding energies of 42, 39, and 36 MeV and at a laboratory angle of 9.75°. These three energies cover the range of interest for the recoiling compound nuclei of the fused systems, and no significant energy dependence of the transmission probability was observed over this range. In order to investigate how strongly the transmission depends on the mass of the analyzed products, we also used a ^{81}Br beam at 45 and 42 MeV; no measurable mass dependence was noted. We define the transmission probability as the ratio of the number of particles detected at the SSB detector to that initially traveling within the solid angle determined by the entrance slit of the

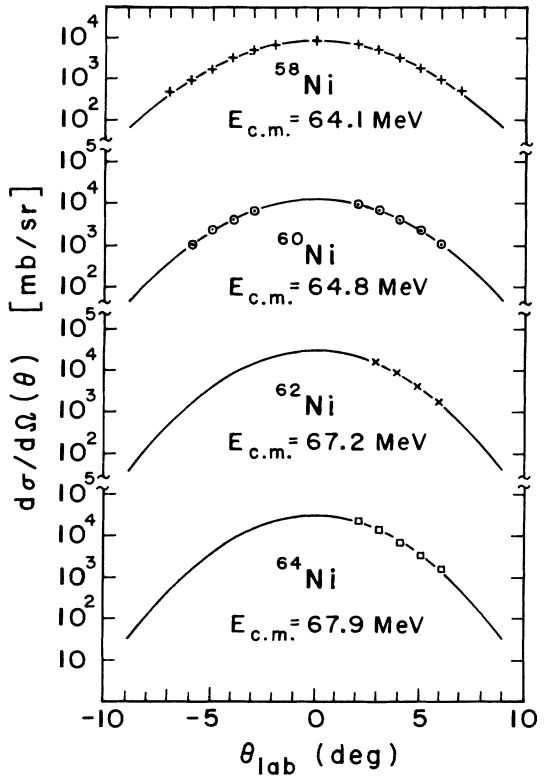

FIG. 1. Experimental angular distributions and corresponding Gaussian fits for ^{37}Cl+^{58,60,62,64}Ni at c.m. energies of 64.1, 64.8, 67.2, and 67.9 MeV, respectively. In each case, the error bars are smaller than the size of the symbols.

TOF arm (58 μsr). The experimental value of the transmission probability, $T=0.780\pm0.045$, was confirmed by measuring the ^{35}Cl+^{58}Ni reaction which was previously analyzed by Scobel *et al.*,[8] using a different experimental technique. For this purpose, an angular distribution of ^{35}Cl+^{58}Ni evaporation residues was obtained at a bombarding energy of 100.33 MeV, which after correcting for energy loss in the target corresponds to a center-of-mass (c.m.) energy of 62.1 MeV. The value obtained for the integrated fusion yield was 44.0±1.4 mb, in excellent agreement with the value of 46.9±4.7 mb reported in Ref. 8.

As a final check on our transmission determinations, a Monte Carlo model was used to simulate the performance of the spectrometer under different operating conditions. A detailed report of this study will appear elsewhere. Here it can be said that, as a result of this theoretical analysis, it is known that the transmission is not strongly dependent on any parameters other than the electrostatic rigidity E/q of the ion and the voltage on the deflector. Fortunately, even the latter dependence is weak and the transmission is stable against±5% deviations in the applied voltage.

In a preliminary experiment, it was determined that the shape of the ER angular distribution did not change appreciably over the energy range of interest in this work, so that it was sufficient to measure them at convenient energies. Typical angular distributions for all four systems are shown in Fig. 1. Excitation functions for all systems were measured at an angle of $\theta_{lab}=3°$. In order to convert this single angle excitation function into a total fusion yield, the ER angular distributions were fitted with a Gaussian function and then integrated to get the total fusion cross section at one energy, which could be used to deduce the absolute cross sections at other energies. Beam energy losses in the targets were corrected for by an iterative procedure, taking into account the slopes of the excitation function. At each step, corrected beam energies were obtained by weighting the energies from the previous step by the experimental fusion cross section, and averaging over the energy loss in the target. This process was repeated until self-consistent results were obtained. See Ref. 6 for a more detailed account of this procedure.

TABLE II. Total fusion cross sections for ^{37}Cl+^{58,60,62,64}Ni.

System	$E_{c.m.}$ (MeV)	σ_{fus} (mb)
^{37}Cl+^{58}Ni	56.9	0.20(5)
	57.5	0.40(15)
	58.1	0.85(16)
	58.7	2.11(31)
	59.4	5.16(74)
	59.9	13.2(10)
	60.5	22.0(15)
	61.1	35.0(33)
	61.7	54.0(29)
	62.3	68.0(30)
	62.9	90.0(29)
	63.5	125(7)
	64.1	152(7)
	64.7	164(13)
	65.3	174(11)
^{37}Cl+^{60}Ni	57.1	0.09(2)
	57.7	0.31(2)
	58.3	0.90(6)
	58.9	2.71(13)
	59.5	6.49(22)
	60.1	14.0(5)
	60.7	24.8(8)
	61.2	44.0(14)
	61.8	58.0(17)
	62.4	75.0(23)
	63.0	92.0(29)
	63.6	125(4)
	64.2	148(5)
	64.8	178(5)
	65.4	195(6)
	66.1	223(7)
^{37}Cl+^{62}Ni	56.6	0.13(4)
	57.2	0.54(10)
	57.9	3.20(32)
	58.5	7.70(54)
	59.1	20.0(9)
	59.7	34.0(13)
	60.4	54.0(18)
	61.0	74.0(20)
	61.6	99.0(42)
	62.2	129(6)
	62.9	167(8)
	63.5	182(7)
	64.1	211(8)
	64.7	241(10)
	65.4	259(14)
	66.0	300(15)
	66.6	340(15)
	67.2	363(19)
^{37}Cl+^{64}Ni	56.0	0.10(2)
	56.6	0.27(3)
	57.3	1.00(10)
	57.9	3.40(20)
	58.5	8.60(42)
	59.1	16.2(6)
	59.7	33.0(12)
	60.3	47.0(14)
	60.9	72.0(22)
	61.6	90.0(27)
	62.2	104(4)
	62.8	138(6)
	63.3	163(6)
	63.4	171(6)
	64.1	183(6)
	64.7	234(7)
	65.3	244(7)
	66.0	301(11)
	66.6	305(13)
	67.2	332(10)
	67.9	355(11)

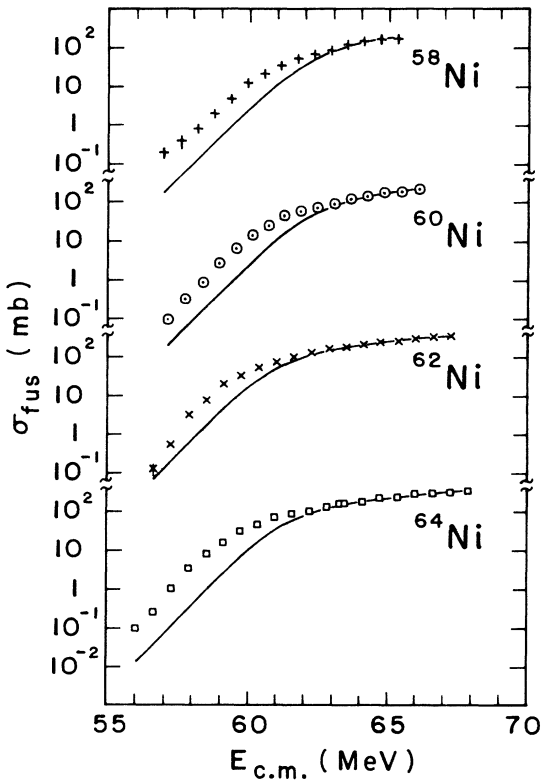

FIG. 2. Experimental total fusion cross sections compared with one-dimensional tunneling-model calculations (solid curves) for the four systems studied.

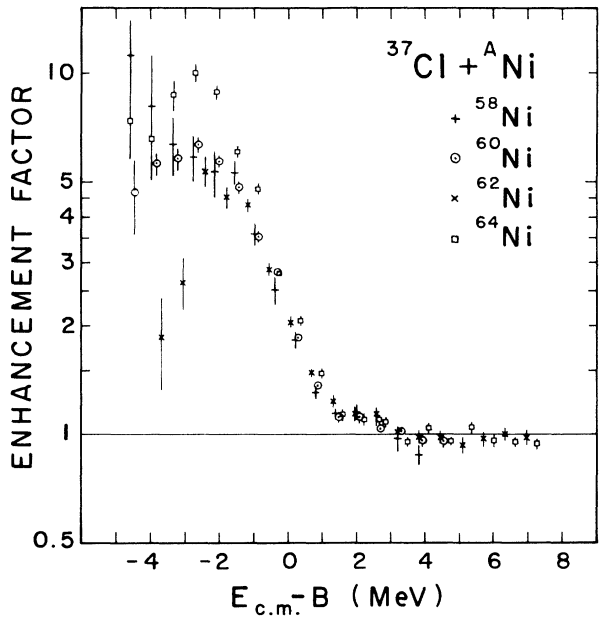

FIG. 3. Enhancement factors relative to the one-dimensional model predictions vs c.m. energy relative to the barriers given in Table III.

The systematic errors associated with the determination of the absolute fusion cross section are estimated to be 8.2%. The principle sources of error are 5.8% from the uncertainty in the transmission measurements, 3.5% from error introduced in the reduction of single-angle cross sections to total cross sections, and finally 4.6% due to angular uncertainty in the positioning of the time-of-flight spectrometer. The total fusion cross sections measured for the four systems are listed in Table II, and plots of these data are shown in Fig. 2. The error bars displayed here do not include the systematic error in the total yield. The solid curves which appear on this figure will be explained below.

At this point, it must be noted that the fusion excitation functions shown in Fig. 2 for $^{37}Cl+^{58,62,64}Ni$ do not agree with the published data of Skorka *et al.*[9] It is for this reason that we made every effort to assure ourselves that the transmission probability through the electrostatic deflector was well understood, without however being able to resolve the discrepancy. On the other hand, the $^{35}Cl+^{58,64}Ni$ fusion excitation functions given in Ref. 9 also do not agree with the earlier results of Scobel *et al.*,[8] and the differences are similar to those we have observed with our own data. As mentioned above, though we measured only one cross section in common with Ref. 8, it agreed to well within the reported errors.

Our experience with ^{181}Ta contamination of one of the targets used in the present experiment (Table I) suggests that similar high-Z contaminant may have been present in the targets of Ref. 8. Such contamination lowers the apparent yield because of the normalization relative to the Rutherford cross section, and the effect is energy dependent. The possibility that the targets used in the experiment reported in Ref. 9 were thicker than anticipated must also be considered, since this could resolve the apparent discrepancies by shifting the excitation functions toward lower energy. Shifts of 1.2 , 1.4, and 0.6 MeV for $^{37}Cl+^{58,62,64}Ni$, respectively, fully account for the differences but seem rather large when one notes that the corresponding shifts in the laboratory energies are 2.0, 2.2, and 1.0 MeV.

TABLE III. Barrier parameters from this work and from systematics (Ref. 3).

	This work			Systematics	
System	V_b (MeV)	R_b (fm)	$\hbar\omega$ (MeV)	V_b (MeV)	R_b (fm)
$^{37}Cl+^{58}Ni$	61.50	10.43	3.79	63.32	10.04
$^{37}Cl+^{60}Ni$	61.52	10.42	3.74	62.94	10.10
$^{37}Cl+^{62}Ni$	60.27	10.66	3.71	62.57	10.16
$^{37}Cl+^{64}Ni$	60.60	10.59	3.67	62.21	10.22

III. RESULTS AND DISCUSSION

In a first attempt to understand the sub-barrier fusion in these systems, we compared our data with the predictions of a one-dimensional tunneling model using the noncoupling mode of the code CCFUS.[10] The potential used in this calculation consisted of a sum of the Coulomb potential for two point charges, plus a centrifugal term and a real nuclear potential having a Woods-Saxon shape. The Schrödinger equation is then solved assuming a black nucleus, so there are no reflections from the nuclear interior, and the fusion cross section is computed from Wong's formula:[11]

$$\sigma_{\rm fus}=(R_b^2/2E_{\rm c.m.})\times\hbar\omega\ln\{1+\exp[(2\pi/\hbar\omega)(E_{\rm c.m.}-V_b)]\}\ . \quad (1)$$

Here, R_b, V_b, and $\hbar\omega$ are the radial position, height, and curvature of the barrier, respectively. The depth of the real part of the nuclear potential, the one free parameter in these calculations, was adjusted in order to fit the data over the cross-section range from 100 to 500 mb. The radius parameter R_b was calculated according to:[12]

$$R_b=R_p+R_t+0.29\ \text{fm}\ , \quad (2)$$

with

$$R_{p,t}=1.233\,A_{p,t}^{1/3}-0.978\,A_{p,t}^{-1/3}\ \text{fm}\ . \quad (3)$$

Here, $p(t)$ refers to the projectile (target) radius. The diffuseness of the nuclear potential was set equal to 0.63 fm as suggested in Ref. 12. The barrier parameters obtained from these calculations are listed in Table III, together with the corresponding values from the systematics established by Vaz Alexander, and Satchler,[3] The agreement is good in the sense that the barrier parameters extracted from our data are within a few percent of the predictions from Ref. 3. A discrepancy of 3% in the barrier height and 4% in its location is apparent, which is within the range of uncertainty (±4%) deduced from the systematic error in our absolute cross sections, and also the ±2% theoretical uncertainty suggested in Ref. 3. While this appears to be only a small disagreement, the effect of such shifts on the predicted cross sections are large due to the exponential dependence on energy relative to the barrier. The discrepancy must also be judged relative to our results for Al+Ge systems[6] where the agreement with Ref. 3 is excellent; the Z_pZ_t product is 416 for this case, nearly equal to the value $Z_pZ_t=476$ for Cl+Ni. Elastic-scattering data on these systems would provide a very useful check on the barrier parameters deduced from the fusion data.

TABLE IV. Spectroscopic and intrinsic quadrupole moments and deformation parameters obtained from Refs. 15–17 and used in the present calculations.

Nucleus	J^π	E_x (MeV)	Q ($e$fm^2)	Q_0 ($e$fm^2)	$\beta^{\rm CCFUS}$
^{37}Cl	$\frac{3}{2}^+$	g.s.	−6.8(1)	−34(5)	−0.18
^{58}Ni	2^+	1.45	−10(6)	35(21)	0.08
^{60}Ni	2^+	1.33	3(5)	−11(18)	−0.02
^{62}Ni	2^+	1.17	5(12)	−18(42)	−0.04
^{64}Ni	2^+	1.35	35(20)	−123(70)	−0.26

TABLE V. Parameters corresponding to vibrational degrees of freedom used in the CCFUS coupled-channels calculation, extracted from Refs. 19 and 20.

Nucleus	J^π	E_x (MeV)	λ	S_λ (W.u.)	$\beta^{\rm CCFUS}$
^{37}Cl	$\frac{1}{2}^+$	1.73	2	2.2	0.14
	$\frac{5}{2}^+$	3.09	2	6.0	0.24
	$\frac{7}{2}^-$	3.10	3	11.1	0.32
	$\frac{9}{2}^-$	4.01	3	12.0	0.33
^{58}Ni	2^+	1.45	2	10.3	0.20
	3^-	4.47	3	12.1	0.21
^{60}Ni	2^+	1.33	2	13.7	0.22
	3^-	4.04	3	10.9	0.19
^{62}Ni	2^+	1.17	2	12.3	0.21
	3^-	3.75	3	13.8	0.22
^{64}Ni	2^+	1.35	2	10.3	0.19
	3^-	3.58	3	14.1	0.22

The fusion excitation functions predicted by the tunneling calculations (Fig. 2), which always underestimate the sub-barrier yield, clearly indicate that the present data cannot be described by a one-dimensional model. In order to facilitate comparison of the individual systems, however, it is convenient to plot the "enhancement factor" over these calculations versus the c.m. energy relative to the barrier (Fig. 3). A number of interesting features emerge from this plot. First of all, a most conspicuous deviation occurs for the two lowest-energy ^{37}Cl+^{62}Ni points, which lie a factor of 2 below the gen-

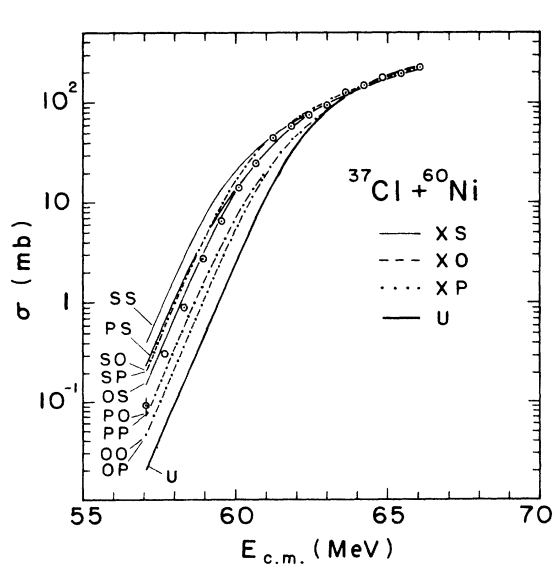

FIG. 4. The ten different predictions for sub-barrier fusion in the ^{37}Cl+^{60}Ni system, compared with the experimental data. See text for an explanation of the symbols.

eral trend for the other systems. The most probable reason for this discrepancy is the small Ta contamination of the target (Table I) which made the normalization to the Rutherford cross section difficult, particularly at the lower energies. Note also the systematic deviation of the $^{37}Cl+^{64}Ni$ yield around 3 MeV below the barrier, which will be shown below to be related to the structure of ^{64}Ni. Finally, a most curious and interesting feature of all the systems studied is the small step in the enhancement factor from 1 to 3 MeV above the barrier, which is not reproduced in any of the calculations we have performed.

We are led by the large enhancement factors shown in Fig. 3 to try to take into account the coupling to additional degrees of freedom, such as the excitation of low-lying states of the projectile and target. To include these inelastic channels, we performed coupled-channels calculations within the strong-coupling scheme, using a modified version of the program CCFUS [13] which allows for both a static rotor description as well as coupling to surface vibrations. The potential used in these calculations, and in particular the depth of its nuclear part, is the same as that used in the one-dimensional calculation. The approach that we have used in this work is to obtain all the relevant nuclear structure information from the literature. In dealing with static deformation, the analysis has been restricted to quadrupole shapes only and the deformation parameter was calculated according to[14]

$$\beta_i=(5\pi)^{1/2}(3Z_t eR_t^2)^{-1}Q_{0i} , \quad (4)$$

where $i=p$ (t) for the projectile (target) and Q_{0i} is the intrinsic electric quadrupole moment obtained from Refs. 15–17. The radius parameter R_i was calculated according to Eq. (3). The dynamic deformation parameter in the case of surface vibrational models is calculated from the corresponding reduced transition probability[18] S_λ via

$$\beta_\lambda^2=4\pi(2\lambda+1)(Z[\lambda+3])^{-2}S_\lambda , \quad (5)$$

where S_λ, expressed in Weisskopf units, was obtained from Refs. 19 and 20. The spectroscopic information is summarized in Tables IV and V.

Although the shape of the nucleus (prolate or oblate) is specified by the sign of the intrinsic quadrupole moment (with positive sign corresponding to prolate deformation), it was decided to carry out the coupled-channels calculation for both shapes, fixing the magnitude to that given in Table IV, in order to test the sensitivity of sub-barrier fusion to the character of the deformation. Thus, for each nucleus we consider three possibilities: static prolate shape (P), static oblate shape (O), and spherical vibrator (S). The set of all ten possible calculations (including the uncoupled case) is shown in Fig. 4 for $^{37}Cl+^{60}Ni$.

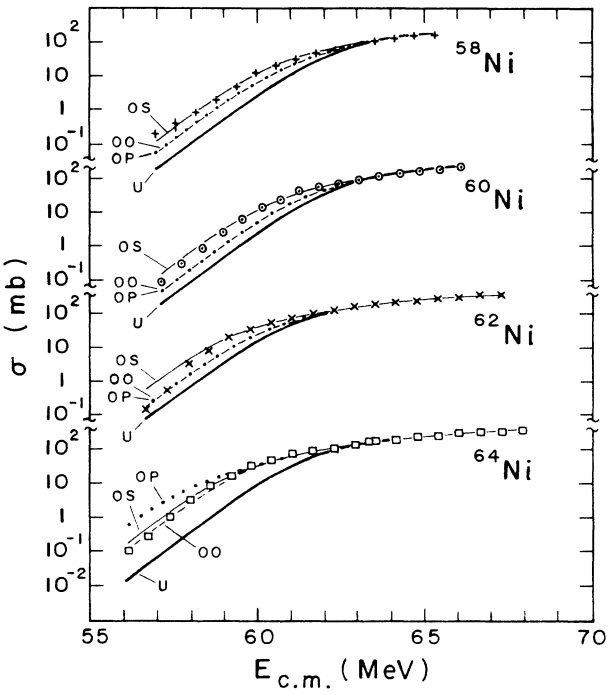

FIG. 5. Experimental fusion cross sections for $^{37}Cl+^{58,60,62,64}Ni$, compared with CCFUS calculations in which ^{37}Cl is assumed to be oblate deformed.

The labels on the curves correspond to the collective nature of the projectile (first letter) and the target (second letter). It is clear that the best representation of the data occurs for the OS combination, which assumes an oblate shape for ^{37}Cl. In order to quantify this observation and compare with the other systems, we computed the χ^2 value for all the calculations, given in Table VI. It can be seen that the minimum value of χ^2 always occurs for an oblate projectile which agrees with the negative sign of the deformation given for ^{37}Cl in Table IV. With respect to the four Ni targets, the χ^2 value reaches its minimum for a spherical shape in the case of the three lighter isotopes. A moderate oblate deformation is favored for ^{64}Ni although the data are also consistent with a spherical vibrational nucleus. Static prolate deformation is clearly ruled out. It is likely that this structural difference between ^{64}Ni and the lighter isotopes accounts for the systematic difference in the enhancement factor for this sys-

TABLE VI. χ^2 values for each of ten different theoretical predictions of the sub-barrier fusion cross section. See text for an explanation of the symbols.

System	OS	OO	OP	PS	PO	PP	SS	SO	SP	U
$^{37}Cl+^{56}Ni$	1.3	10.9	10.7	2.3	7.8	7.8	26	13	13	34
$^{37}Cl+^{60}Ni$	6.6	89	89	42	58	59	304	50	50	188
$^{37}Cl+^{62}Ni$: [a]	2.5	30	31	5.8	25	26	43	10	10	73
$^{37}Cl+^{64}Ni$	8.1	7.0	157	9.5	24	250	40	351	1450	120

[a]Lowest-energy two points excluded. See text.

tem that is apparent in Fig. 3. The quality of the various predictions can easily be judged in Fig. 5, which shows all the calculations corresponding to an oblate shape for the projectile. In particular, note that the OS calculation is preferred for all systems except ^{37}Cl+^{64}Ni, where the OO solution is slightly favored. Note also the disagreement with the two lowest-energy ^{37}Cl+^{62}Ni points which has been remarked on above.

IV. CONCLUSIONS

Fusion excitation functions around and well below the barrier have been obtained for the reactions ^{37}Cl+^{58,60,64}Ni, using an electrostatic deflector in conjunction with a TOF-energy telescope. The measured fusion cross sections covered over three orders of magnitude from 100 μb to 400 mb. We have been unable to confirm the cross sections for some of these systems reported by Skorka *et al.*[9] In general, our measured cross sections are larger at a given energy than those given in Ref. 9.

The experimental data show considerable enhancements when compared with calculations based on a one-dimensional tunneling model. Coupled-channel calculations within the strong-coupling scheme, and considering only inelastic excitation of the lowest-lying states of the target and projectile, were able to reproduce these enhancements quite well using spectroscopic information taken from the literature. In agreement with existing spectroscopic data, the results of our calculations favor moderate oblate deformations for ^{37}Cl and ^{64}Ni, while the three lighter Ni isotopes are best represented as spherical vibrators. Static prolate deformation for either target or projectile is ruled out. On the basis of the good agreement with experiment obtained in the present work, there is no need to invoke particle-transfer degrees of freedom[9] as significant contributers to the sub-barrier fusion yield for any of the systems studies. Finally, one interesting unexplained systematic feature of our data is a small step in the enhancement factor which occurs just above the barrier.

ACKNOWLEDGMENTS

We would like to thank Dr. S. Landowne for fruitful discussion on the coupled-channels calculations, and for providing us with the latest version of the code CCFUS. We also gratefully acknowledge R. Kryger, S. Graff, and Dr. R. J. Vojtech, and Dr. J. D. Hinnfeld for their generous help during the data acquisition. This work was supported by the U.S. NSF under Contract Nos. INT88-03658 and PHY88-03035, and by the Consejo Nacional de Ciencia y Tecnológia (Mexico) under Contract No. 140105 G102-139.

*Present address: Department of Physics, University of Notre Dame, Notre Dame, IN 46556.

†Present address: Centre de Recherches Nucleaires and Universite Louis Pasteur, 67037 Strasbourg CEDEX, France.

‡Present address: Institute of Nuclear Research, Academia Sinica, P.O. Box 8204, Shanghai 201849, People's Republic of China.

[1]N. F. Ramsey, Phys. Rev. **83**, 649 (1951); G. Breit, M. H. Hull, and R. L. Gluckstern, Phys. Rev. **87**, 74 (1952).

[2]See references in Proceedings of the Symposium on The Many Facets of Heavy-Ion Fusion Reactions, Argonne National Laboratory Report ANL-PHY-86-1, 1986.

[3]L. C. Vaz, J. M. Alexander, and G. R. Satchler, Phys. Rep. **69**, 373 (1981).

[4]M. Beckerman, Phys. Rep. **129**, 145 (1985); Rep. Prog. Phys. **51**, 1047 (1988); S. G. Steadman and M. J. Rhoades-Brown, Ann. Rev. Nucl. Part. **36**, 649 (1986).

[5]J. J. Vega, E. F. Aguilera, G. Murillo, and J. J. Kolata, Notas Fis. **10**, 335 (1987).

[6]E. F. Aguilera, J. J. Vega, J. J. Kolata, A. Morsad, R. G. Tighe, and X. J. Kong, Phys. Rev. C **41**, 910 (1990).

[7]E. F. Aguilera, J. J. Vega, E. Martinez, J. J. Kolata, and A. Morsad, Rev. Mex. Fis. **35**, 489 (1989).

[8]W. Scobel, H. H. Gutbrod, M. Blann, and A. Mignerey, Phys. Rev. C **14**, 1808 (1976).

[9]S. J. Skorka, A. M. Stefanini, G. Fortuna, R. Pengo, W. Meczynski, G. Montagnoli, A. Tivelli, S. Beghini. C. Signorini, and P. R. Pascholati, Z. Phys. A **328**, 355 (1987).

[10]C. H. Dasso, S. Landowne, and A. Winther, Nucl. Phys. **A405**, 381 (1983); R. A. Broglia, C. H. Dasso, S. Landowne, and G. Pollarolo, Phys. Lett. **133B**, 34 (1983).

[11]C. Y. Wong, Phys. Rev. Lett. **31**, 766 (1973).

[12]P. R. Christensen and A. Winther, Phys. Lett. **65B**, 19 (1976); R. A. Brolia and A. Winther, *Heavy Ion Reactions* (Benjamin, New York, 1981), Vol. 1.

[13]J. Fernandez-Niello, C. H. Dasso, and S. Landowne, Comp. Phys. Comm. **54**, 409 (1989).

[14]J. P. Davidson, *Collective Models of the Nucleus, Pure and Applied Physics* (Academic, New York, 1968), Vol. 29, p. 107.

[15]M. Elbel and R. Quad, Z. Naturforsch. **41A**, 15 (1986).

[16]P. M. S. Lesser, D. Cline, P. Goode, and R. N. Horoshko, Nucl. Phys. **A190**, 597 (1972).

[17]P. Raghavan, At. Data. Nucl. Data Tables **42**, 189 (1989).

[18]R. A. Broglia and F. Barranco, in *Fusion Reactions Below the Barrier*, Vol. 219 of Lecture Notes in Physics, edited by S. G. Steadman (Springer-Verlag, Berlin, 1985), p. 182.

[19]J. Albinski, A. Budzanowski, H. Dabrowski, Z. Rogalska, S. Wiktor, H. Rebel, D. K. Srivastava, C. Alderliesten, J. Bojowald, W. Oelert, C. Mayer-Böricke, and P. Turek, Nucl. Phys. **A455**, 477 (1985).

[20]P. M. Endt, At. Data Nucl. Data Tables **23**, 547 (1979).